Available online at www.sciencedirect.com
SCIENCE DIRECT®
Renewable Energy 29 (2004) 2167–2181
RENEWABLE ENERGY
www.elsevier.com/locate/renene

Performance optimization of a photovoltaic induction motor pumping system

A Betka [a,*], A. Moussi [b]

[a] *Electrical Engineering Institute, University of Oum El Bouaghi, 04000 Oum El Bouaghi, Algeria*
[b] *Larhyss Laboratory, University of Biskra, Biskra, Algeria*

Received 9 October 2002; accepted 26 March 2004

Abstract

The performances of a photovoltaic pumping system based on an induction motor are degraded once insolation varies far from the value called nominal, where the system was sized. To surmount this handicap, an improvement of these performances by the optimization of the motor efficiency is described in this paper. The results obtained are compared with those of similar work pieces presented in the literature where the motor effeciency and air gap flux where optimized separatly. The simulation results show that the proposed system allows at the same time to combine the performances of the system with constant efficiency and the simplicity of implementation provided by the system with constant airgap flux.

Keywords: Photovoltaic system; Induction motor; Optimization; Efficiency

1. Introduction

Photovoltaic pumping is receiving more attention in recent years especially in remote areas where connection to the grid is technically not possible or economically unaffordable. Such systems operate in open-loop speed control because precision and transient performance are not required. In addition the system operates at steady state for long periods. Various studies have been carried out on sizing [3,6], matching [9,10] and optimizing [20] PV systems. DC motors were initially used since they offered easy implementation with cheap power conversion [4,5,17–19]. A number of existing operational pumping systems have shown that these schemes suffer

* Corresponding author. Fax: +355-213-032-42-23-85.
E-mail address: a_Betka@hotmail.com (A. Betka).

0960-1481/$ - see front matter
doi:10.1016/j.renene.2004.03.016

Nomenclature

V	output generator voltage (V)
I	generator current (A)
I_{cc}	short-circuit current (A)
V_{th}	thermic voltage (V)
I_o	reverse saturation current (A)
R_s	series generator resistance (Ω)
I_{op}	optimum generator current (A)
V_{op}	optimum generator voltage (V)
V_{oc}	open circuit voltage (v)
P_M	maximum (optimum) generator power (w)
E	insulation (w/m^2)
$V_m$rms	motor voltage (V)
r_1	stator resistance per phase (Ω)
r_2	equivalent rotor resistance per phase (Ω)
r_m	core loss resistance (Ω)
x_1	stator leakage reactance (Ω)
x_2	equivalent rotor leakage reactance (Ω)
x_m	magnetizing reactance (Ω)
x_{11}	stator cyclic reactance (Ω)
x_{22}	rotor cyclic reactance (Ω)
ω_s	angular frequency of the supply (rd/s)
ω_{sl}	slip speed (rd/s)
p	pair pole number
ω	motor speed (rd/s)
f	motor frequency (Hz)
H	total head (m)
H_g	geodetic head (m)
Q	flow rate (m^3/h)
ρ	water volumic mass (kg/m^3)
g	gravity acceleration (m/s^2)
C	constant which depends on pump nominal data
T_o	friction coefficient
a_0, a_1, a_2	constants depending on the pump dimensions
t_{sr}	sunrise time (chosen as $t_{sr} = 8:00$)
t_{ss}	sunset time (chosen as $t_{ss} = 18:00$)

from maintenance problems. To overcome this drawback, brushless permanent magnet DC motors have been proposed [2]. However, this solution is limited only for low power PV systems. The induction motor based PV pumping system offers an alternative for a more reliable and maintenance free systems [16]. In addition, recent advances in the field of solid state devices, logic circuits and control theory have

given a great impetus to the use of AC motors in PV systems. Several papers report AC systems using either current source or voltage source inverters. Different optimization strategies have been proposed to improve the overall system efficiency such as maximum power tracking or MPPT [11,12,15,16], motor efficiency optimization [13,21] and flowrate maximization [1].

In this paper an optimal operation of a direct photovoltaic pumping system based on an induction motor is presented. The optimization problem consists of improving the motor efficiency by the minimization of a non-linear criterion. This is achieved by a proper adjustment of the frequency and the modulation index of the PWM voltage source inverter feeding the motor. It is in fact functioning under airgap flux weakening.

As a benchmark for the subsequent results, works presented in Refs. [21] and [14] are used. Yao found that by a proper adjustment of the inverter frequency, a constant optimum value of the motor efficiency is ensured, while maximum power of the PV generator is made available to the load by a DC/DC converter operating as a maximum power point tracker. Even if an optimal motor efficiency is preserved in Yao et al. [21], the conservation of the DC/DC power stage makes the implementation more expensive. This handicap was discarded by Duzat [14], leading therefore to less implementation complexity. In contrary to Yao et al. [21], the generator output voltage is no longer controlled by the MPPT, but with a linear relationship which relates this voltage to the inverter frequency. However, the preservation of a constant airgap flux for light torque loads (centrifugal pumps) in Duzat [14], leads to an increase of iron losses under weak solar insolation where motor efficiency degradation is noticed.

In this paper, a field weakening operation deducted from the optimization of a non-linear criterion provides at the same time the high performances of Yao et al. [21] and implementation simplicity of Duzat [14]. The schematic diagram of the proposed system is shown in Fig. 1. It consists of a photovoltaic generator, a PWM voltage source inverter and an induction motor driving a monocellular centrifugal pump. The paper will model each component of the system prior to

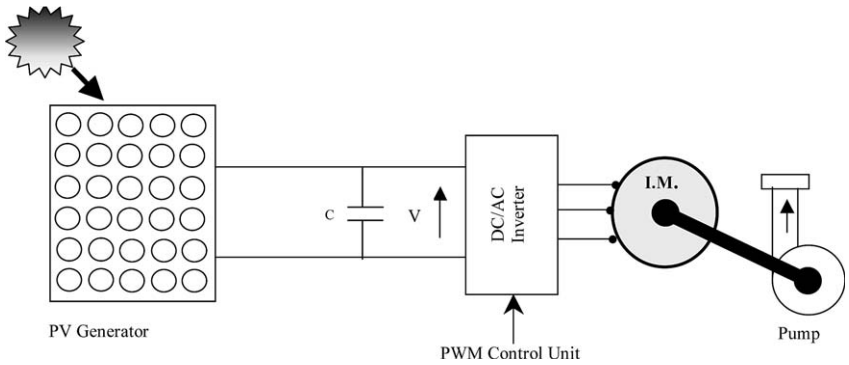

Fig. 1. The PV scheme structure.

presentation of the results through simulation. In the derivation of the system equations, some assumptions are made. The motor is supposed to be unsaturated and unaffected by the harmonic effects of the inverter. The power losses in the inverter and stray losses in the motor are also supposed negligible. Furthermore, dynamic equations are not considered since the system is assumed to run in steady state. The rest of the paper is organized in four sections. In Section 2 various parts of the system are modelled. The proposed optimization criterion is presented in Section 3. Simulation results and interpretations are presented in Section 4.

2. Modelling of the PV system

The proposed PV system is composed of the solar array, the VS inverter, the induction motor, the centrifugal pump and pipelines. The mathematical model for individual parts is described in the following section.

2.1. PV generator model

The PV generator considered in this study is a 16 series connected modules type AEG.40. The I-V characteristic can be written as:

$$I = I_{sc} - I_0 . \left(\exp\left(\frac{V + R_S I}{V_{th}} \right) - 1 \right) \tag{1}$$

The adaptation of Eq. (1) for different levels of solar insolation can be obtained by the following equations described in Moussi et al. [1]:

$$I_{sc} = I_{sc\ r} . \left(\frac{E}{E_r} \right) \tag{2}$$

$$V_{oc} = V_{oc\ r} + V_{th} \ln\left(\frac{E}{E_r} \right) \tag{3}$$

$$I_0 = \frac{I_{sc}}{\exp\left(\frac{V_{oc}}{V_{th}} \right) - 1} \tag{4}$$

where the suffix r refers to rated conditions given by $E = 1000\ \mathrm{W/m^2}$ and $T = 25\ ^\circ\mathrm{C}$.

The use efficiency of the generator is identified by the ratio of the power extracted by the load to the maximum power available:

$$\eta_{use} = \frac{VI}{P_M} \tag{5}$$

2.2. Inverter model

A natural PWM switching technique is used to drive the DC-AC inverter with a modulation index M and the ratio between the frequencies of the carrier and modulating waveforms P. It can be shown from Murphy and Turnbull [7] that in the

case of a full bridge control and for $P > 9$, the rms value of the fundamental motor voltage V_{m} is given by:

$$V_m = \frac{MV}{\sqrt{2}} \tag{6}$$

For the case studied in Yao et al. [21], the modulation index is set to: $M = 0.8$.

2.3. Three phase induction motor model

The steady state performance of the induction motor is modelled using the conventional equivalent circuit shown in Fig. 2

From Fig. 2 it can be shown that the electrical input power is given by:

$$P_{\mathrm{in}} = 3R_{\mathrm{eq}} \frac{V_{\mathrm{m}}^2}{Z_{\mathrm{eq}}^2} \tag{7}$$

Z_{eq} is the equivalent input impedance per phase:

$$Z_{\mathrm{eq}} = R_{\mathrm{eq}} + jX_{\mathrm{eq}} \tag{8}$$

The mechanical equation is defined as:

$$T_e = T_r + T_0 \ \omega \tag{9}$$

where the electromagnetic torque T_e is given by Murphy and Turnbull [7]:

$$T_e = 3p\left(\frac{V_m}{\omega_s}\right)^2 \frac{\omega_{\mathrm{sl}} \dfrac{x_m^2}{r_2}}{\left[r_1 - \dfrac{\omega_{\mathrm{sl}}}{\omega_{\mathrm{s}} r_2}\left(x_{11}x_{22} - x_m^2\right)\right]^2 + \left[x_{11} + \dfrac{\omega_{\mathrm{sl}} r_1 x_{22}}{\omega_{\mathrm{s}} r_2}\right]^2} \tag{10}$$

and T_r is the centrifugal pump load torque given by an aerodynamic equation in the form:

$$T_r = C\left(1 - \frac{\omega_{\mathrm{sl}}}{\omega_{\mathrm{s}}}\right)^2 \omega_s^2 \tag{11}$$

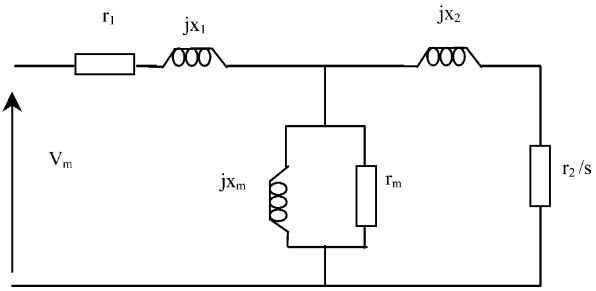

Fig. 2. Steady-state equivalent circuit.

2.4. Centrifugal pump model

The head-flowrate H-Q characteristic of a monocellular centrifugal pump is obtained using Pfleider-Peterman model [1]. The multispeed family head-capacity curves are shown in Fig. 3 and can be expressed approximately by the following quadratic form:

$$H = a_0\omega^2 + a_1\omega Q + a_2 Q^2 \tag{12}$$

where the motor speed ω is expressed as:

$$\omega = \left(1 - \frac{\omega_{sl}}{\omega_s}\right)\omega_s \tag{13}$$

The pump efficiency is defined as the ratio of the hydraulic power imparted by the pump to the fluid to the shaft mechanical power and is given by:

$$\eta_p = \frac{\rho\ g\ H\ Q}{C\left(1 - \frac{\omega_{sl}}{\omega_s}\right)^3 \omega_s^3} \tag{14}$$

The H-Q characteristic of the pipe network can be expressed by:

$$H = H_g + \psi Q^2 \tag{15}$$

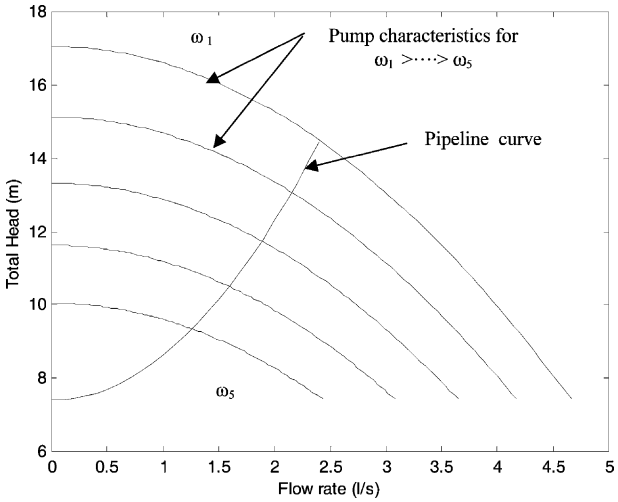

Fig. 3. Pump H-Q characteristics.

2.5. Insolation model

A simplified approach was elaborated according to Khousem and Khousem [8], and which will serve as a first aproximative quantification of the incidental inso-

lation. This model quantifies irradiance for a standard clear day:

$$E = E_M \sin(15.(t - t_{sr}))\frac{\pi}{180} \tag{16}$$

3. Proposed approach

In case of constant airgap flux operation exposed by Duzat [14], although it offers acceptable results in the electric plan (see Fig. 9), and in the hydraulic plan, as shown in Fig. 5, the motor efficiency, which is displayed in Fig. 4, falls considerably for weak insolation levels as a result of an increase of iron losses. In this paper, an improvement of this efficiency using a variable airgap flux operation is proposed. This is reached by the optimization of a non-linear criterion representing the motor efficiency and by varying two degrees of liberty:

- The inverter frequency f and
- Modulation index M.

For implemetation, f indicates the frequency of the modulation waveform.

In contrary to Yao et al. [21], the generator voltage, and hence the electric power extracted from the generator, is controlled by the strategy exposed by Duzat [14] where a linear relationship between this voltage and frequency can be expressed:

$$V = C_{10} + C_{11} f \tag{17}$$

In the generator I-V plan and under Eq. (17), the system may operate in three intervals:

(a) $V < V_{op} \quad Pe < P_M$
(b) $V = V_{op} \quad Pe = P_M$
(c) $V > V_{op} \quad Pe < P_M$

It was shown in Olorunfemi [13] that case (a) corresponds to an unstable motor operation since the motor speed presents a non-minimum phase response and highly oscillating evolutions of ω are noticed. Case (b) implies the use of the MPPT [21]. In this study, the last case is adopted since stable operation is ensured [14]. In order to avoid operation in case (a), constant C_{10} should be greater than V_{op} for low frequencies. However C_{11}, which gives the curve slope, should not be too small in order to avoid operating away from maximum power for high insolation values.

For the present study, constants are chosen as follows:

$$C_{10} = 240 \ \ V\left(\text{corresponding to } V_{op} \text{ of } E = 100 \ \text{w/m}^2\right)$$

$$C_{11} = 0.4.$$

The ideality of the inverter allows the power balance equation of the system to be defined as:

$$\left(V_{th}\ln\left(\frac{I_{sc} - I + I_o}{I_o}\right) - IR_s\right)I = 3\frac{R_{eq}}{Z_{eq}^2}V_m^2 \tag{18}$$

3.1. Optimization criterion

For an improvement of the motor efficiency, the momentary value of the following vector must be determined:

$$X = [\omega_{sl}\, f \;\; I \;\; M]^{T} \tag{19}$$

Minimizing the objective function:

$$J = -f(X) \tag{20}$$

where $f(X)$ is the motor efficiency given by:

$$f(X) = \frac{C\left(1 - \dfrac{\omega_{sl}}{2pif}\right)^{3} (2pif)^{3}}{\left(V_{th}\ln\left(\dfrac{I_{sc} - I + I_{o}}{I_{O}}\right) - IR_{s}\right) I} \tag{21}$$

Associated to the equality constraints:

$$g(X) = 0 \tag{22}$$

formed by the set of Eqs. (9), (17) and (18).

In addition, the generator current I and the modulation index M are limited as:

$$0 \le I \le I_{cc} \tag{23}$$

$$0 \le M \le 1 \tag{24}$$

3.2. Optimization method

The resolution of the constrained problem (20) is carried out by the function 'FMINCON' from the software 'MATLAB'. This is generally referred to as constrained non-linear optimization. It uses the sequential quadratic programming (SQP) algorithm which represents the state-of-the art in non-linear programming methods.

At each iteration, the constrained problem, Eqs. (20), (22), (23) and (24) are transformed to an other unconstrained problem with linearized constraints using the Lagrangian function which is solved by the quadratic programming algorithm:

$$L(X, \lambda) = -f(X) + \sum_{i=1}^{m} \lambda_i G_i(X) \tag{25}$$

where G contains at the same time the equality and inequality constraints (Eqs. (22), (23) and (24)). λ_i $(i = 1, \ldots\ m)$ are Lagrange multipliers and m is the number of all constraints. The Hessian matrix updating is made by the formula of Broyden, Fletcher, Goldfarb and Shanno (BFGS) [22].

After performing optimization, the daily pumped water quantity is defined as:

$$D = \int_{t_{sr}}^{t_{ss}} Q \, \mathrm{d}t \tag{26}$$

4. Simulation results

The simulation is undertaken on a system characterised by the data given in the Appendix. Figs. 4–9 show the system performances for reference temperature $T = 25\ ^{\circ}\mathrm{C}$ using the proposed approach and compared to those given by Yao et al. [21] and Duzat [14]. Fig. 4 depicts the motor efficiency as a function of solar insolation. It is seen that an optimal efficiency $\eta_m = 0.73$ can be maintained constant using the appropriate optimization technique. The control law given by Eq. (20) mainly governs the reduction of losses which are frequency dependent (iron and friction losses), which represents a superiority with regard to the constant airgap flux system [14] in particular for the weak values of insolation ($E < 650\ \mathrm{w/m^2}$), while the algorithm presented in Yao et al. [21] produces similar results where a motor efficiency value $\eta_m = 0.71$ is maintained by variation of the motor frequency.

Fig. 5 shows clearly the pump flow rate, based on head values, obtained by equating Eq. (12) and Eq. (15). The pump succeeds in overcoming geodetic head H_g and starts pumping at low insolation level, $E = 320\ \mathrm{w/m^2}$, for the proposed approach and that described by Yao et al. [21]; whereas the constant flux mode [14] does not start to deliver water unless solar insolation exceeds $360\ \mathrm{w/m^2}$. This increase of the flow rate is due to the proportionality between mechanical power on the shaft of a centrifugal pump and flowrate [1]. The improvement of the mechanical power and hence of the flowrate are obtained by the maximization of the

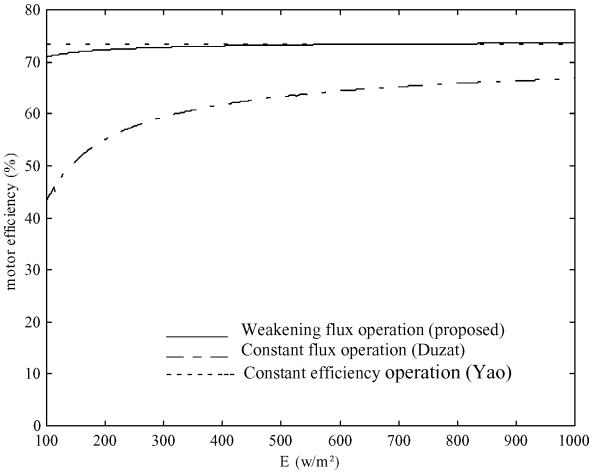

Fig. 4. Induction motor efficiencies.

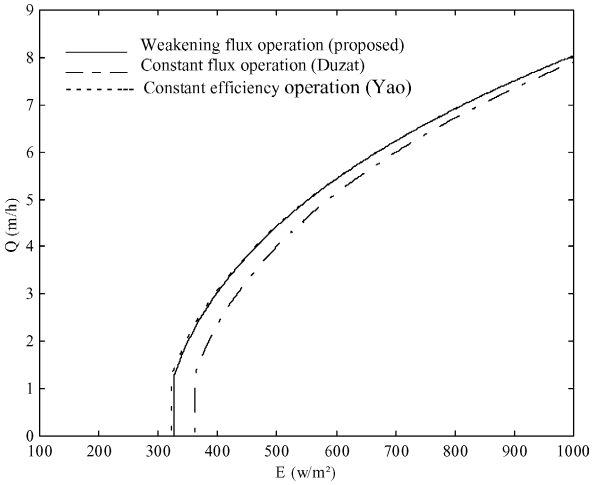

Fig. 5. Pump flow-rate characteristics.

motor speed via the optimization criterion. Consequently, this increase of the pump flowrate leads to an elevation of the daily pumped quantity. By adopting the model of insolation described by Eq. (16), and according to numerical integration of Eq. (26), the daily amount of pumped water is:

- 28.84 m^3 for the constant air gap flux technique [14].
- 31.14 m^3 for the system described in Yao et al. [21].
- 31.00 m^3 with the proposed approach.

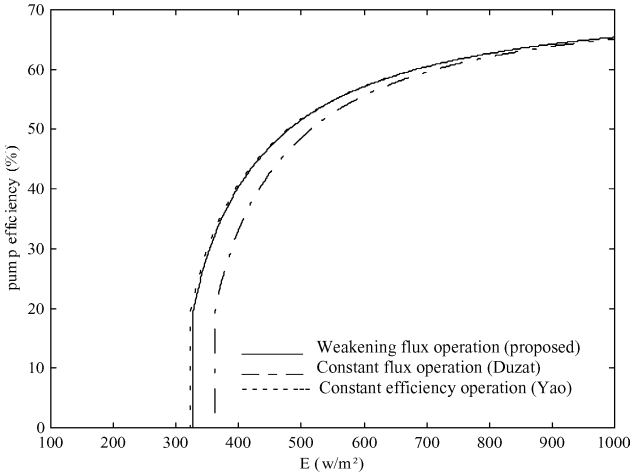

Fig. 6. Pump efficiencies.

Fig. 6 displays the improvement brought to the pump efficiency by the proposed technique. It can be seen that an improvement of this efficiency was carried out with the proposed approach, as well as that described in Yao et al. [21]. Compared with Duzat [14], this increase is greater for the weak values of insolation ($E < 650$ w/m^2), and inflicts the two following parameters:

- An increase of the total head H given by Eq. (12) as a result of the friction and shock losses reduction inside the pump.
- An increase of the flowrate Q as a result of the leakage flow-rate decrease [14].

Consequently, the hydraulic power ($\rho \times g \times H \times Q$) is enhanced.

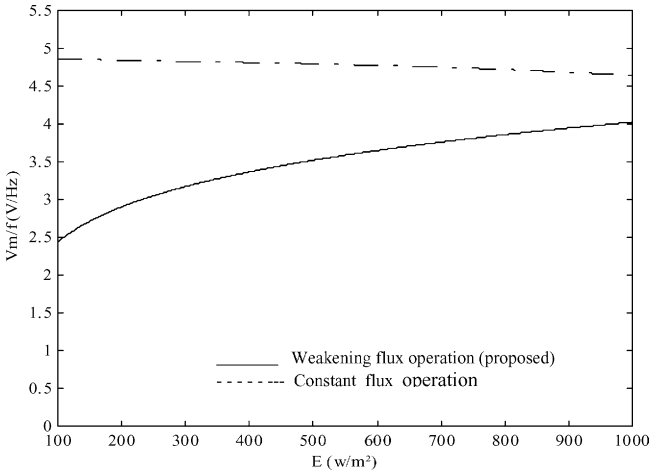

Fig. 7. Airgap flux characteristics.

Fig. 7 illustrates the airgap flux, represented by the quotient (V_m/f), for the proposed approach, and that described in Duzat [14]. One can notice that the improvement of the motor efficiency is obtained with a field weakening, which is more noticeable for weak insolation values (corresponding to light torque loads). This flux reduction leads essentially to a decrease in the motor iron losses. On the other hand, for the Duzat [14], a nominal flux value is maintained permanently constant ($V_m/f \cong 4.8$).

Fig. 8 shows the generator power–voltage characteristics and maximum power locus together with the consumed power in the case of constant airgap flux mode [14], and field weakening mode that is proposed in our study, while Fig. 9 illustrates the generator use efficiency characteristic. It is clear that for these two cases, the power consumed by the system is very close to that maximal absorbed by the system [21] for high insulation values, and does not deviate significantly for lower values, bearing in mind that the MPPT block is omitted. This leads to use

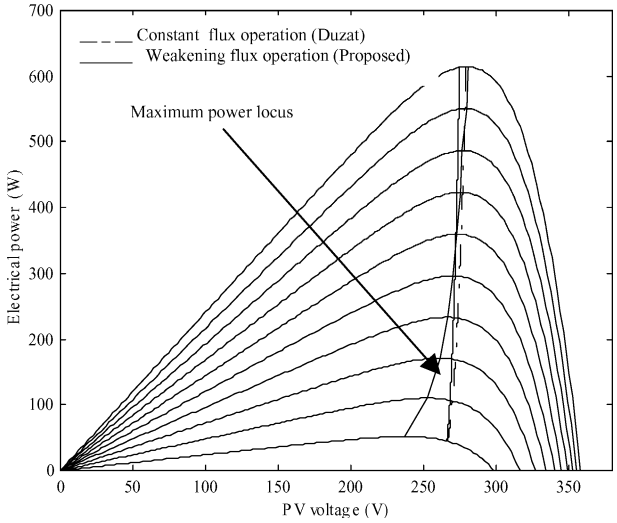

Fig. 8. Operating power point locus for different insulation levels.

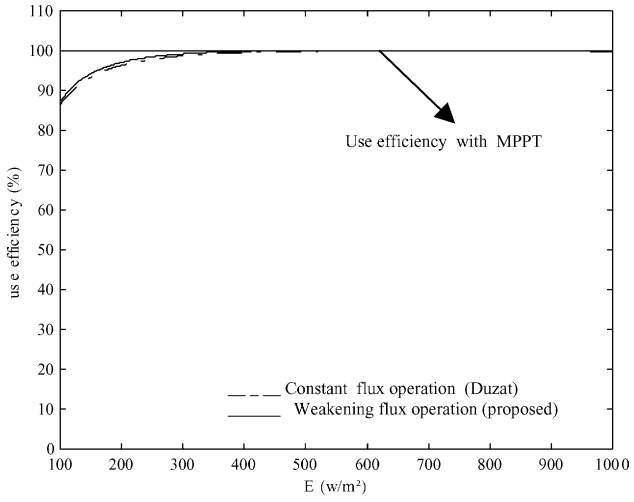

Fig. 9. Use efficiency curves.

efficiency values $\eta_{use} > 98\%$ for all insulation levels. Consequently, the implemetation will be less complex, less expensive and more reliable.

In Fig. 10a the modulation index M is presented, while Fig. 10b illustrates the inverter frequency f. One notices that the modulation index is reduced once the frequency falls, bringing consequently a decrease of the motor voltage V_m since the generator voltage is approximately constant (see Fig. 8). As a result, the airgap flux is reduced.

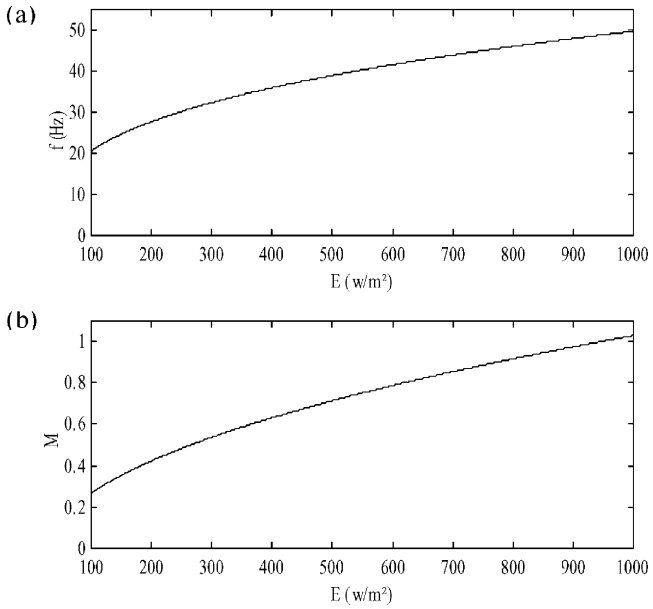

Fig. 10. Modulation index and frequency curves.

5. Conclusion

An optimal operation of a direct photovoltaic pumping system based on an induction motor was described. The optimization criterion fixes the maximization of the motor efficiency, and where the extracted electric power is controlled by the inverter frequency instead of MPPT. A comparative study was carried out on two systems described in Yao et al. [21] and Duzat [14]. The simulation results show that an increase of both the daily pumped quantity and pump efficiency are reached by the proposed approach. In addition, the generator voltage control law leads to a less expensive and non-complex implemetation. Thus the advantages described are acquired meanwhile overriding their inconvenience.

Acknowledgements

The authors wish to thank the staff of the department of electrical engineering of the University of Nottingham for the facilities provided and valuable suggestions in improving this work.

Appendix

PV generator parameters:

Type AEG	for $E = 1000$ w/m^2 and $T = 25\ ^\circ$C
Maximum power	614.24 W

Optimal current	2.2 A
Optimal Voltage	279.2 V
Open circuit voltage	358.4 V
Short circuit current	2.41 A

Induction motor parameters:

$V = 380$ V	$I = 2.5$ A	$P = 1$ kW
$x_1 = x_2 = 15.7\ \Omega$	$r_1 = 22.5\ \Omega$	$r_2 = 7.87\ \Omega$
$x_m = 586\ \Omega$	$r_m = 1.127$ K Ω	

Centrifugal pump parameters:

$H = 14$ m	$Q = 2.59$ l/s	
$P = 521$ W	$N = 3000$ tr/mn	
Pipe network:	$\varnothing = 0.06$ m	$H_g = 7.4$ m

References

[1] Moussi A, Betka A, Azoui B. Optimum design of photovoltaic pumping system. Leicester, UK: UPEC99; 1999.

[2] Swamy CLP, et al. Dynamic performance of a permanent magnet brushless DC motor powered by a PV array for water pumping. Solar Energ Mat Solar Cell 1995;36:187–200.

[3] Shrertha GB, Goel L. A study on optimal sizing of stand alone photovoltaic stations. IEEE Trans Energ Conv 1998;13(4):373–7.

[4] Appelbaum J. Starting and steady state characteristics of DC motor powered by solar cell generator. IEEE Trans Energ Conv 1986;1(1):17–25.

[5] Appelbaum J, Sarme MS. The operation of permanent magnet DC motors powered by a common source of solar cells. IEEE Trans Energ Con 1989;4(4):635–42.

[6] Samin J, et al. Optimal sizing of photovoltaic systems in varied climates. Solar Energ 1997;6(2):97–107.

[7] Murphy JMD, Turnbull FG. Power electronics control of AC motors. Pergamon Press; 1985.

[8] Khousem K, Khousem L. Optimum matching of direct-coupled electromechanical loads to a photovoltaic generator. IEEE Trans Energ Conv 1993;8(3).

[9] Akbaba M, et al. Matching of separately excited DC motors to photovoltaic generators for maximum power output. Solar Energ 1998;63(6):375–85.

[10] Saied MM. Matching of DC motor to photovoltaic generator for maximum daily gross mechanical energy. IEEE Trans Energ Conv 1988;3(3):465–71.

[11] Eskandar MN, Zaki AM. A maximum efficiency photovoltaic-induction motor pump system. Renew Energ 1997;10(1):53–60.

[12] Veerachary M, Yadaiah N. ANN based peak power tracking for PV supplied DC motors. Solar Energ 2000;69(4):343–50.

[13] Olorunfemi O. Analyses of current source induction motor drive fed from photovoltaic energy source. IEEE Trans Energ Conv 1991;6(1):99–106.

[14] Duzat R. Analytic and experimental investigation of a photovoltaic pumping system, PhD thesis, Oldenburg University 2000.

[15] Alghuwainem SM. Steady state operation of DC motors supplied from photovoltaic generators with step up converters. IEEE Trans Energ Conv 1992;7(2):267–71.

[16] Bhat SR, et al. Performance optimisation of induction motor-pump system using photovoltaic energy source. IEEE Trans Ind App 1987;23(6):995–1000.
[17] Singer S. Starting characteristics of direct current motors powered by solar cells. IEEE Trans Energ Conv 1993;8(1):47–52.
[18] Mummadi VC. Steady state and dynamic performances analysis of PV supplied DC motors fed from intermediate power converter. Solar Energ Mat Solar Cell 2000;61:365–81.
[19] Fam WZ, Balachander MK. Dynamic performances of a DC shunt motor connected to a photovoltaic array. IEEE Trans Energ Conv 1988;3(3):613–7.
[20] Weiner D, Levinson A. Water pumping optimal operation. Elect Mach Power Syst 1996;24(3):277–88.
[21] Yao Y, Bustamente P, Ramshaw RS. Improvement of induction motor drive systems supplied by photovoltaic arrays with frequency control. IEEE Trans Energ Conv 1994;9(2).
[22] Fletcher R. A new approach to variable metric algorithms. Computer J 1970.